Geochimica et Cosmochimica Acta 349 (2023) 1–10

Contents lists available at ScienceDirect

Geochimica et Cosmochimica Acta

journal homepage: www.elsevier.com/locate/gca

Shock-induced potassium and zinc isotope fractionation in ordinary chondrites and its implications

Ying-Kui Xu [a,b,c], Zhi Li [a,d], Shi-Jie Li [a,b,*], Ze-Zhou Wang [c], De-Liang Wang [a,d], Yan Fan [a,e], Xiong-Yao Li [a,b], Jian-Zhong Liu [a,b], Dan Zhu [f,b]

[a] Center for Lunar and Planetary Sciences, Institute of Geochemistry, Chinese Academy of Sciences, Guiyang 550081, China
[b] CAS Center for Excellence in Comparative Planetology, Hefei 230022, China
[c] Isotope Laboratory, Department of Earth and Space Sciences, University of Washington, Seattle, WA 98195, USA
[d] University of Chinese Academy of Sciences, Beijing 100049, China
[e] Department of Geology, Northwest University, Xi'an 710069, China
[f] State Key Laboratory of Ore Deposit Geochemistry, Institute of Geochemistry, Chinese Academy of Sciences, Guiyang 550081, China

ARTICLE INFO

Article history:
Received 8 July 2022
Accepted 25 March 2023
Available online 30 March 2023
Associate editor: Frederic Moynier

Keywords:
Meteorites
Potassium isotopes
Zinc isotopes
Impact
Kinetic

ABSTRACT

To constrain how impacts influence the behavior of moderately volatile elements (MVEs), we report potassium (K) and zinc (Zn) contents and isotopic compositions of shock melt pockets (SMPs) and unmelted parts of three heavily shocked ordinary chondrites and bulk rocks of Chelyabinsk meteorite. All SMPs are enriched in K content and have lower isotopic values ($\delta^{41}K$ = −1.99‰, −1.22‰ and −1.40‰) while the adjacent unmelted parts are enriched in heavy K isotopes ($\delta^{41}K$ = −0.41‰, −0.01‰ and 0.04‰) compared to the bulk rocks of Chelyabinsk meteorite ($\delta^{41}K$ = −0.77‰ and −0.73‰). By contrast, Zn is depleted in SMPs and the isotopic compositions are heavier ($\delta^{66}Zn$ = −0.19‰, 2.42‰, 1.74‰) in SMPs than that in unmelted parts ($\delta^{66}Zn$ = −0.65‰, 1.76‰, −0.97‰). Our results indicate a decoupling between the two MVEs that Zn is lost from shock melts while K is dramatically enriched in shock melts during impacts. The isotope fractionation of Zn is probably caused by evaporation of shock melts, while K isotope fractionation is most likely caused by solid-melt diffusion which is controlled by its incompatibility. The isotopic decoupling of K from Zn during major impacts further enhances our understanding of high temperature elemental and isotopic behavior of MVEs and may shed new light on the variously heterogeneous distribution of MVEs in solar system.

1. Introduction

The heterogeneous distribution of volatile elements remains a mystery in solar system evolution. Terrestrial planets are variably depleted in volatile elements compared with solar photosphere and CI chondrites. Such depletion has been attributed to either nebular processes, e.g., incomplete volatile condensation (Wasson and Chou, 1974; Wai and Wasson, 1977; Humayun and Clayton, 1995; Ciesla, 2008), or planetary processes, e.g., accretion evaporation/condensation (Albarede, 2009; Paniello et al., 2012; Pringle et al., 2014; Wang and Jacobsen, 2016a; Hin et al., 2017; Pringle and Moynier, 2017) and magma ocean degassing (Day and Moynier, 2014; Kato et al., 2015; Gargano et al., 2020). Isotope geochemistry of volatile elements provides the possibility to understand volatile depletion in terrestrial planets since volatile element loss triggers large isotope fractionation. Both potassium (K) and zinc (Zn) are moderately volatile elements, which have 50% condensation temperatures (50% T_c) of 1006 K and 726 K respectively at 10^{-4} bars (Lodders, 2003). With the development of high-precision measurement of K and Zn isotopes (Maréchal et al.,1999; Moynier et al., 2011; Moynier and Le Borgne, 2015; Li et al., 2016; Wang and Jacobsen, 2016b; Hu et al., 2018), large differences in K and Zn isotope compositions among extraterrestrial bodies have been revealed (Luck et al., 2005; Moynier et al., 2007; Herzog et al., 2009; Moynier et al., 2011; Paniello et al., 2012; Chen et al., 2013; Pringle et al., 2017; Brugier et al., 2019; Tian et al., 2019; Bloom et al., 2020; Ku and Jacobsen, 2020; Tian et al., 2020; Zhao et al., 2020; Tian et al., 2021; Nie et al., 2021; Hu et al., 2022; Koefoed et al., 2022; Savage et al., 2022; Steller et al., 2022). Impact events are ubiquitous in solar system and are critical for the formation of planetary bodies of various sizes (Wetherill, 1980; Canup, 2004; Johnson et al., 2016), delivery of

* Corresponding author at: Center for Lunar and Planetary Sciences, Institute of Geochemistry, Chinese Academy of Sciences, Guiyang 550081, China.
E-mail address: lishijielpsc@mail.gyig.ac.cn (S.-J. Li).

https://doi.org/10.1016/j.gca.2023.03.031
0016-7037/

water to the inner solar system (Daly and Schultz, 2018), and shaping of the surface features of extraterrestrial bodies (Nabiei et al., 2018). The shock-induced pressure could exceed 90 GPa, which is hardly achieved in laboratory experiments for hand-specimen scale samples (Fritz et al., 2017). The shock-induced temperatures could be higher than 2000 °C and generate in situ rock melting in the form of shock melt pockets (SMPs) or shock melt veins (SMVs) (Stoffler et al., 1991). Whether impact processes cause K isotope fractionation is yet not clear. Jiang et al. (2019) observed no variation in K concentrations and $\delta^{41}K$ of tektites, which are thought to be the production of high-energy meteoroid impacts. Zhao et al. (2020) and Bloom et al. (2020) measured whole-rock K isotope compositions of chondrites with different shock stages and observed little systematic K isotope variations. By contrast, the evaporative loss and isotopic variation of Zn in shock meteorites and tektites have been reported (Moynier et al., 2009, 2010; Brugier et al., 2019; Jiang et al., 2019). And same conclusions occur in the shock-related terrestrial samples (Kamber and Schoenberg, 2020; Mathur et al., 2021). Considering that all these studies were based on comparison of different types of bulk rocks, the possible isotope fractionations and heterogeneity of K and Zn might be masked at small scale.

Here, we report K and Zn isotopes, whole-rock chemistry, petrology and mineralogy of eight shocked chondritic samples. The eight samples include three pairs of fragments picked from the SMPs and adjacent unmelted parts from Chelyabinsk (LL group), Viñales (L group), and Tassédet 004 (H group), one SMV/SMP free Chelyabinsk fragment, and one whole-rock powder of Chelyabinsk fragment containing SMVs and unmelted parts (Fig. 1). Our study aims to reveal the important role of shock melting events on variations of the isotope composition among extraterrestrial bodies.

2. Materials and methods

2.1. Samples

For petrographic investigation, three slices of Chelyabinsk, Viñales, and Tassédet 004 that contain SMPs and normal lithologies (no visible SMP) were selected and made as polished thick sections, labeled as Che-IG-1, Vin-IG-1, and Tas-IG-1, respectively (Figs. S1–S3). For element and isotope composition measurements, eight samples (Che #1, Che #2, Che #3, Che #4, Vin #1, Vin #2, Tas #1 and Tas #2) were picked from different parts of Chelyabinsk, Viñales, and Tassédet 004 (Fig. 1). The detailed sample information is listed in Table 1.

The Chelyabinsk meteorite (LL5) fell in 2013 in Chelyabinsk, Russia. The shock degree of this meteorite is S5 according to the criteria of Stoffler et al. (1991). One light-colored (without visible SMPs) fragment was labelled as Che #1 and it represents the initial bulk composition of Chelyabinsk meteorite (Fig. 1a); one slice with network SMPs was labelled as Che #2 and represents the whole-rock composition of meteorite that experienced shock melting (Fig. 1b); Che #3 and Che #4 are samples picked separately from the neighbouring (approximately 1 cm in distance) normal lithology (no visible SMPs) and SMP of the same meteorite slice (Fig. 1c).

The L6 ordinary chondrite Viñales fell in 2019 in Cuba, which suffered a shock intensity of S3–S4 (Yin and Dai, 2021). Vin #1 and Vin #2 are picked from the nearby normal lithology and SMP of one Viñales chondrite slice, respectively (Fig. 1d).

The H5-melt breccia ordinary chondrite Tassédet 004 was found in 2016 in Niger. The meteorite suffered slight terrestrial weathering and a high degree of shock (Meteoritical Bulletin Database). Tas #1 and Tas #2 (Fig. 1e) are samples picked from the adjacent normal lithology and SMP of one Tassédet 004 slice. Since metal and troilite in SMP combine to form larger nodules, the color of SMP is slightly lighter than that of normal lithology.

2.2. Methods

2.2.1. Petrographic observation and mineral composition measurement

Petrographic investigations were performed at the Center for Lunar and Planetary Sciences, Institute of Geochemistry, Chinese Academy of Sciences, with a Scios-FIB field emission scanning electron microscope (SEM). Minerals and glass in melting pockets and unmelted parts of the three thick sections were analysed on a JXA8530F-Plus electron microprobe at the State Key Laboratory of Ore Deposit Geochemistry, Institute of Geochemistry, Chinese Academy of Sciences. The accelerating voltage was 25 kV, and

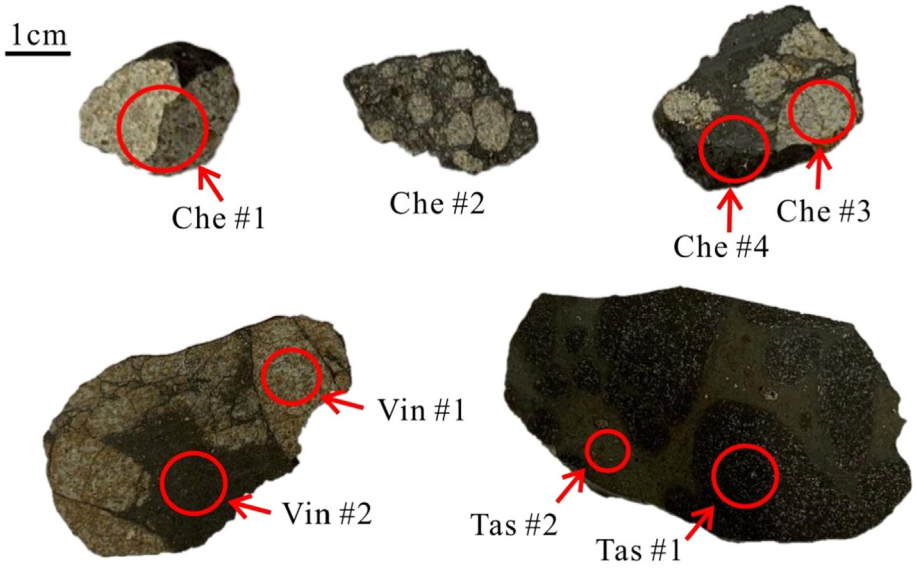

Fig. 1. Studied samples information. Che #1 and #2 represent the bulk composition of Chelyabinsk meteorite (the external melting crust was polished away before we crushed and ground it to powder); Che #3 and #4 are unmelted parts and SMPs picked from Chelyabinsk meteorite; Vin #1 and #2 are the unmelted part and SMPs picked from Viñales meteorite; Tas #1 and #2 are unmelted parts and SMPs picked from the Tassédet 004 meteorite.

Table 1
Major and trace elements for SMPs and unmelted parts of Chelyabinsk, Viñales and Tassédet 004 chondrites.

Sample name	Chelyabinsk				Viñales		Tassédet 004	
	Che #1	Che #2	Che #3	Che #4	Vin #1	Vin #2	Tas #1	Tas #2
Sample description	Bulk rock	Bulk rock	Unmelted region	SMP	Unmelted region	SMP	Unmelted region	SMP
Find/Fall	Fall				Fall		Find	
Type	LL5				L6		H5	
Chemical composition								
Al (wt.%)	1.16	1.20	1.30	1.12	1.02	1.08	0.80	1.16
Ca (wt.%)	1.64	1.76	1.70	1.67	1.12	1.17	1.05	1.32
Fe (wt.%)	21.57	19.83	18.88	21.54	27.88	21.12	34.69	21.61
Mg (wt.%)	14.46	14.58	14.33	14.27	12.59	14.27	11.46	14.58
Mn (μg/g)	2620	2630	2610	2450	2160	2490	1900	2450
Na (μg/g)	6920	7250	7380	6830	6400	6150	4590	6850
P (μg/g)	990	800	860	790	850	980	1560	1020
Ti (μg/g)	650	650	680	790	560	600	480	650
K (μg/g)	938	930	872	1002	712	866	546	974
Li (ug/g)	1.84	1.79	1.81	2.13	1.26	2.64	1.37	2.01
Rb (μg/g)	3.45	3.41	2.55	3.26	2.93	2.90	1.62	2.64
Cu (μg/g)	80.50	156.00	102.00	89.60	134.00	92.30	104.00	53.30
Zn (μg/g)	53.80	49.70	57.50	52.60	39.50	44.50	34.90	40.80
U (ng/g)	10	12	12	13	9	11	21	52

The uncertainties of Na, Mg, K, Ca and Fe are lower than 0.1%; the uncertainties of trace elements are ~10%. SMP = shock melt pocket.

the beam current was 10nA. For olivine and pyroxene, a spot diameter of 10 μm was adopted, while for minor plagioclase and silicate glass, a 1–2 μm spot was chosen. Standards from the SPI Supplies, Inc., USA, were used for data calibration. Elemental line scanning and map scanning were performed by energy spectrum analysis on SEM and electron microprobe, respectively. A Raman spectrometer at the Center for Lunar and Planetary Sciences, Institute of Geochemistry, Chinese Academy of Sciences was used for plagioclase phase identification.

2.2.2. Major and trace elements measurements

The eight samples were processed in a class 100 laminar flow fume hood in a class 10,000 clean laboratory at Guizhou Tongwei Analytical Technology Co., Ltd. Approximately 50–100 mg of rock powder samples were dissolved with a mixture of concentrated nitric acid and hydrofluoric acid in Bomb at 185 °C in an oven for 3 days and dried on a hot plate at 80 °C. Major elements were determined by inductively coupled plasma optical emission spectroscopy (ICP-OES) at the State Key Laboratory of Ore Deposit Geochemistry, Institute of Geochemistry, Chinese Academy of Sciences. Trace elements were measured by using a Thermo Fisher inductively coupled plasma mass spectrometry (ICP-MS) X2 at Guizhou Tongwei Analytical Technology Co., Ltd. The accuracy and precision were monitored by analyses of three geostandards (GSR-3 for major element and BHVO-2 and W-2a for trace element). The uncertainties of major elements and trace elements are lower than 2% and 10%, respectively. Detailed analytical information for trace elements can be found in Li et al. (2021).

2.2.3. Potassium isotope measurements

The K isotopic compositions were measured at the Isotope Laboratory of the University of Washington, Seattle, following the procedure of Hu et al. (2018) and Xu et al. (2019). Briefly, 10–30 mg of sample powders were digested in Teflon beakers using a mixture of HF-HNO_3 (optima-grade, 3:1 v/v). Then, the samples were dried and treated with aqua regia (HCl-HNO_3, 3:1 v/v) and further concentrated HNO_3 until all the samples were completely dissolved. Finally, the solutions were dried and dissolved in 0.5 N HNO_3 for purification. Purification of K was achieved by cation-exchange chromatography. A Bio-Rad Poly-Prep polyethylene column was packed with 2 mL precleaned Bio-Rad AG50 W-X8 resin. After conditioning, the sample solutions were loaded on the resin and eluted with 0.5 N HNO_3. Matrix elements were rinsed off by 13 mL 0.5 N HNO_3, and the subsequent 22 mL fraction K solution was collected. The column procedure was repeated twice to achieve an effectively pure K solution.

The K isotopes were measured on a Nu Plasma II multi-collector inductively coupled plasma mass spectrometry (MC-ICPMS) in high mass resolution mode. Lowered RF power and "dry plasma" were used to suppress interferences from isobaric argides. Potassium isotope analysis was achieved on the interference-free peak shoulder. Instrumental mass fractionation was corrected by the sample-standard bracketing (SSB) method. The K isotopic composition is expressed in delta (δ) notation relative to the National Institute of Standards and Technology (NIST) Standard Reference Materials (SRM) 3141a: $\delta^{41}K = [(^{41}K/^{39}K)_{sample}/(^{41}K/^{39}K)_{standard} - 1] \times 1000$. The uncertainties are reported as 2SD (standard deviation) [see published paper (Hu et al., 2018) for details]. The error-weighted average K isotopic values and uncertainties were reported for those samples with duplicate analysis.

In addition to the meteorite samples, a geological reference material (BHVO-1) was prepared and processed through the whole procedure during K isotope determination to monitor the accuracy of the meteorite K isotope data. The BHVO-1 yield a value of −0.37 ± 0.07‰ (n = 4), consisting well with previous reported value ($\delta^{41}K_{BHVO-1}$ = −0.41 ± 0.02‰) (Xu et al., 2019).

2.2.4. Zinc isotope measurements

The Zn purification was performed at the State Key Laboratory of Ore Deposit Geochemistry, Institute of Geochemistry, Chinese Academy of Sciences, following the method of Zhu et al. (2018). ~100 mg samples were individually transferred to a 15-mL Teflon digestion vial and then reacted with concentrated HNO_3 and HF until samples were completely dissolved. After evaporation to dryness and re-dissolution in 2 N HCl, the solutions were transferred into a 15 mL polypropylene centrifuge tube. Purification of Zn was achieved on columns containing 3 mL of pre-cleaned 100–200 mesh AG MP-1 M anion-exchange resin. After the adsorption of metals onto the column, 30 mL of 2 N HCl was passed through the columns. Zn was eluted using 12 mL of 0.012 N HCl. The solution was evaporated to dryness at 110 °C and dissolved in 3 mL of 1% HNO_3. Additionally, the final solution (0.5 mL) was used for Zn content measurements to monitor the recoveries, and the residue

was used for Zn isotope composition analysis. Satisfactory recoveries were obtained (>98%).

The Zn isotopic compositions were measured on a Thermo Scientific Neptune Plus MC-ICPMS instrument, the State Key Laboratory of Crust Mantle Evolution and Mineralisation at Nanjing University. Instrumental mass bias correction of Zn isotopes was achieved through a coupled method of sample-standard bracketing (SSB) and Cu doping. In this study, Zn isotopic ratio is expressed in standard delta (δ) notation relative to the IRMM 3702 Zn solution during measurements: $\delta^{66,68}Zn = [(^{66,\ 68}Zn/^{64}Zn)_{sample}/(^{66,\ 68}Zn/^{64}Zn)_{standard}-1] \times 1000$. As Zn fractionation in our samples was mass-dependent, only $\delta^{66}Zn$ is discussed.

At present, the Johnson Matthey (JMC) Zn 'Lyon JMC 3-0749L solution' is the most widely used bracketing Zn standard when reported Zn isotope data. Thus, the measured Zn isotopic data are corrected to those relative to the JMC standard using the equation $\delta^{66}Zn_{JMC} = \delta^{66}Zn_{IRMM\ 3702} + 0.28‰$ (Wang et al., 2017). A rock standard (BCR-2) was processed through the whole procedure during Zn isotope determination and it yields an average $\delta^{66}Zn_{JMC}$ = 0.20 ± 0.03‰ (n = 3), consisting well with previous reported values ($\delta^{66}Zn_{JMC}$ = 0.25 ± 0.03‰; Moynier et al., 2017). A solution of Zn isotope standard (CAGS-1) analyzed during the course of this study yields an average of $\delta^{66}Zn_{JMC}$ = 0.58 ± 0.02‰, agreeing well with the literature values (0.56 ± 0.03‰, Zhu et al., 2018; 0.59 ± 0.05 ‰, Yang et al., 2022).

3. Results

3.1. Petrology and mineralogy

The slice of the Chelyabinsk meteorite (labeled as Che-IG-1) has two different ocular parts: light and dark (Fig. S1a). The light part (unmelted) has a typical type 5 lithology. Fractures are dense in olivine and pyroxene grains, and tiny shock melt veins and melted plagioclases are common (Fig. S1b–c). The dark part (melted) consists of the silicate melted fraction and the darkening fraction (Fig. S1b). In the darkening fraction, the majority of fractures are filled with troilite, sometimes with FeNi metal (Fig. S1b–e). The silicate melted fraction (Fig. S1d–f) shows a porphyritic texture composed of large relic olivine (20–300 μm, ~15 vol%), small recrystallized olivine and pyroxene (mostly less than 10 μm), which are cemented in silicate glass, and troilite and Fe-Ni metal spherical assemblages.

The slice of the Viñales meteorite (Vin-IG-1) consists of brown (normal) and dark parts (Fig. S2a). Both parts are highly fractured and some of the plagioclase grains are altered to maskelynite (Fig. S2b–c). The dark part is composed of silicate SMVs and darkening fractions (Fig. S2b, d).

The SMP in Tassédet 004 (Tas-IG-1) is in a delta shape between two normal unmelted parts (Fig. S3a). The Tassédet 004 is more porous than the Chelyabinsk and Viñales meteorites (Fig. S3a, c). The unmelted parts of Tas-IG-1 are significantly affected by shock events, given tiny SMVs are observed; many cracks are filled with melted plagioclase; and troilite dots are commonly present in olivine and pyroxene grains (Fig. S3b–c). The texture and mineral assemblage of SMP in Tas-IG-1(Fig. S3d) is similar to that of Che-IG-1 except the silicate glass is much lower in Fe and Mg contents.

In the unmelted parts, K is mainly enriched in plagioclase/-maskelynite, while in melt pockets, silicate glass and plagioclase glass are the main K-bearing phases (K_2O = 0.1 wt% – 1.4 wt%). Olivine and pyroxene contain little K (K_2O < 0.01 wt%) (Table S1). For the Che-IG-1 and Vin-IG-1, K contents in plagioclase and silicate glass are variable but no clear trend was observed. Notably, for Tas-IG-1, plagioclase glass in SMP display higher K contents than plagioclase in unmelted parts (Table S1).

3.2. Bulk chemistry

Major and trace elemental concentrations of the eight samples are reported in Table 1. The K concentrations of three SMPs are higher than that of their paired unmelted parts. The K contents of Che #1 and #2 are 938 and 930 μg/g, respectively, with a mean value of 934 μg/g, representing the bulk-rock K content. The K content of Che #4 (SMP) is 1002 μg/g, while the K content of Che #3 (unmelted part) is 872 μg/g. The K contents of Vin #1 (unmelted part) and #2 (SMP) are 712 and 866 μg/g, respectively; the K contents of Tas #1 (unmelted part) and #2 (SMP) are 546 and 974 μg/g, respectively. To eliminate the systematic deviation caused by iron variations, ratios of magnesium-normalized abundances of SMPs and unmelted parts are plotted in Fig. S4. Zinc is depleted in SMPs compared to that in unmelted parts after Mg normalization. In addition to K and Zn, other elements also show variations between SMPs and unmelted parts, e.g., lithium is enriched while copper is depleted in SMPs (Fig. S4).

3.3. Potassium and zinc isotopic compositions

The K and Zn isotopic data are reported in Table 2 and plotted in Fig. 2.

The SMV-free Chelyabinsk sample (Che #1) has a $\delta^{41}K$ value of −0.77 ± 0.03‰. The bulk Chelyabinsk sample (Che #2) that experienced shocked melting has a $\delta^{41}K$ value of −0.73 ± 0.10‰, identical to that of Che #1. In comparison, the three SMPs (Che #4, Vin #2 and Tas #2) have much lower $\delta^{41}K$ values ($\delta^{41}K_{Che\ \#4}$ = −1.99 ± 0.14‰, $\delta^{41}K_{Vin\ \#2}$ = −1.22 ± 0.09‰, $\delta^{41}K_{Tas\ \#2}$ = −1.40 ± 0.06‰), whereas the unmelted samples (Che #3, Vin #1 and Tas #1) have much higher values ($\delta^{41}K_{Che\ \#3}$ = −0.41 ± 0.09‰, $\delta^{41}K_{Vin\ \#1}$ = −0.01 ± 0.10‰, $\delta^{41}K_{Tas\ \#1}$ = 0.04 ± 0.02‰).

The $\delta^{66}Zn$ of Che #1 and Che #2 are 0.20 ± 0.02‰ and 0.06 ± 0.09‰, respectively. The $\delta^{66}Zn$ of Che #4 is 0.09 ± 0.01‰, heavier than that of Che #3, −0.37 ± 0.04‰. Vin #2 from melt pocket has higher Zn isotopic value ($\delta^{66}Zn_{Vin\ \#2}$ = 2.70 ± 0.02‰) relative to the unmelted part Vin #1 ($\delta^{66}Zn_{Vin\ \#1}$ = 2.04 ± 0.02‰). Tas #2 from melt pockets also shows higher $\delta^{66}Zn$ values of 2.02 ± 0.06‰ than unmelted part Tas #1 ($\delta^{66}Zn_{Tas\ \#1}$ = 1.25‰).

4. Discussion

Both K and Zn shows elemental and isotopic variations between SMPs and unmelted parts. Below, we first discuss the possible mechanism and processes that caused these variations, then explore the implication for MVEs heterogeneity in the inner solar system.

4.1. K isotopic fractionation during heavy shocks

Overall, K isotopic composition becomes lighter with increasing K content (Fig. 3a). To eliminate the influence of heterogeneous distribution of plagioclase, we plotted $\delta^{41}K$ versus K/Al (Fig. 3b), since plagioclase is the major carrier mineral for K and Al in ordinary chondrites. The evident correlations of $\delta^{41}K$ versus K contents and K/Al ratio strongly indicate that K has migrated to the SMPs, while Al remain in the unmelted parts during impact melt events. Two pathways that might account for K migration are discussed below: (1) migration of K via evaporation, or (2) via melt-solid diffusion.

4.1.1. Evaporation induced K migration and isotopic fractionation

Since K is a moderately volatile element, it could evaporate during high-temperature processes, which was confirmed by previous experiments (Yu et al., 2003; Neuman et al., 2022). Chen and

Table 2
Sample description, K and Zn isotopic compositions of study samples and geological reference material.

Sample	Description	K (μg/g)	δ^{41}K (‰)	2SD	n	Zn (μg/g)	Zn/Mg	δ^{66}Zn $_{IRMM\ 3702}$ (‰)	δ^{66}Zn $_{JMC}$ (‰)	2SD	n
Che #1	Bulk rock	938	−0.73	0.10	4	53.8	3.721	−0.08	0.20	0.02	2
Duplicate			−0.78	0.04	3						
Average			−0.77	0.03							
Che #2	Bulk rock	930	−0.73	0.10	6	49.7	3.409	−0.22	0.06	0.09	2
Che #3	Unmelted	872	−0.41	0.09	6	57.5	4.012	−0.65	−0.37	0.04	2
Che #4	SMP	1002	−1.99	0.14	6	52.6	3.686	−0.19	0.09	0.01	2
Vin #1	Unmelted	712	−0.01	0.10	7	39.5	3.139	1.76	2.04	0.02	2
Vin #2	SMP	866	−1.22	0.09	6	44.5	3.118	2.42	2.70	0.02	2
Tas #1	Unmelted	546	0.01	0.03	4	34.9	3.046	0.97	1.25	0.00	2
Duplicate			0.10	0.05	3						
Duplicate			0.07	0.03	2						
Average			0.04	0.02							
Tas #2	SMP	974	−1.40	0.06	6	40.8	2.799	1.74	2.02	0.06	2
BHVO-1	Basaltic geostandard		−0.37	0.07	4						
Duplicate			−0.41	0.11	5						
Duplicate			−0.40	0.10	5						
BCR-2	Basaltic geostandard							−0.08	0.20	0.03	3

Notes. Unmelted: samples without shock melt characteristic under naked eye. SMP: shock melt pocket. Duplicate: repeat analyses on the same sample during different sessions.

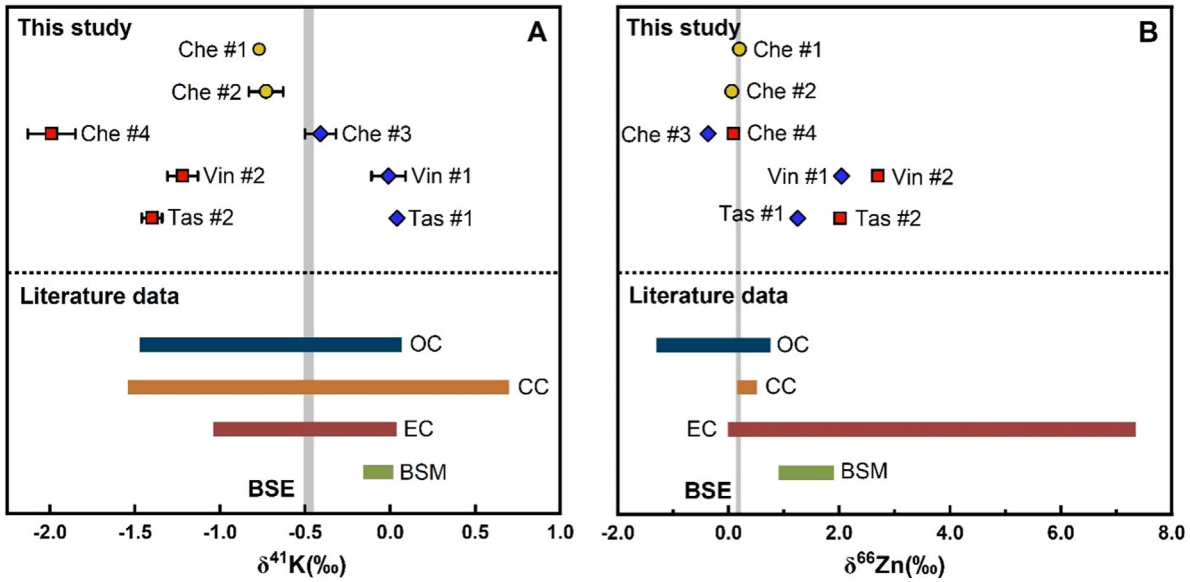

Fig. 2. K and Zn isotopic compositions of studies meteorites and comparison with data from literatures. (A) δ^{41}K values of SMPs are systematically lower than those of corresponding unmelted parts. δ^{41}K values of bulk silicate Earth (BSE), bulk silicate Moon (BSM), ordinary chondrites (OC), carbonaceous chondrites (CC) and enstatite chondrite (EC) are quoted from published papers (Bloom et al., 2020; Tian et al., 2020; Zhao et al., 2020; Nie et al., 2021). (B) δ^{66}Zn values of SMPs are systematically higher than those of paired unmelted parts. δ^{66}Zn values of BSE, BSM, OC, CC and EC are quoted from published papers (Luck et al., 2005; Barrat et al., 2012; Sossi et al., 2018; Yang et al., 2021).

Goresy (2000) observed K enrichment in maskelynite, and they proposed K evaporated from shock veins and subsequently "scavenged" by plagioclase-like melt pockets, yet the underlying mechanism for such a K "scavenge" is not clear. However, the observed K migration in our study is not likely caused by evaporation. The reasons are listed below: (1) If evaporation controls the migration, Na should also show an enrichment in SMPs since it has even lower 50% T_c than K, yet the Na enrichment was not observed (Fig. S4). (2) Lithium, which has a 50% T_c of 1142 K, was also enriched in SMPs, indicating that the evaporation temperature is not the controlling factor. (3) Importantly, the normal interpretation of the evaporation process should be that K evaporates from the hot melting region and condenses in cold unmelted regions, which is opposite to our observation.

4.1.2. Diffusion of K to SMPs via solid-melt reaction

Alternatively, melt-solid diffusion of K could be the possible path. The driving force for K diffusion is its partitioning between minerals and melts before the equilibrium is reached, as K is a highly incompatible element and prefers melts even compared with K-bearing minerals, e.g., plagioclase (Aigner-Torres et al., 2007). Since impact-induced melting is an extremely fast process (milliseconds), i.e., the coexisting melt and solid are completely out of equilibrium with each other at the initial time, K in plagioclase will tend to transport toward the SMPs by diffusion (Fig. 4). This transport process will lead the SMPs to be enriched in light K isotopes, leaving the residual solid phase with isotopically heavy K. As a comparison, Na is a compatible element with even lower 50% T_c (900 K) than K. No enrichment of Na in SMPs indicates that

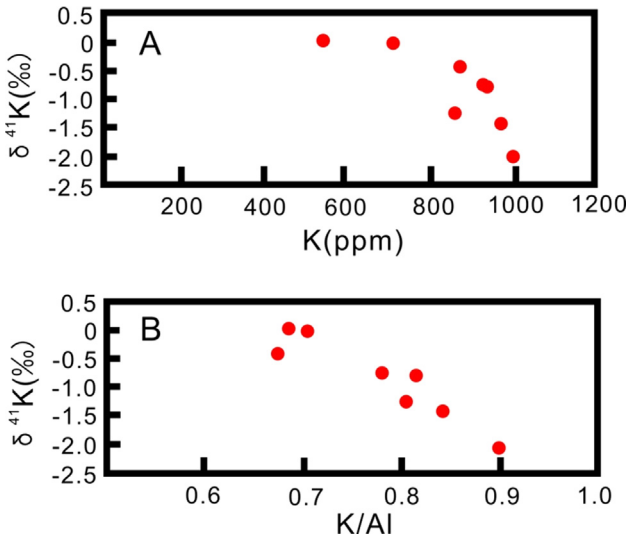

Fig. 3. K isotope compositions versus the K contents and K/Al ratios for all eight samples. (A) and (B) indicate that $\delta^{41}K$ decreases with increasing K contents and K/Al ratios. The correlations of $\delta^{41}K$ versus K contents and K/Al ratios strongly indicate that K isotopic fractionation is the result of K migration related kinetic isotopic effect, leaving the Al in situ.

it is the geochemical affinity controls the migration rather than the condensation temperature.

The diffusing distance was evaluated under the situation of "simple diffusion model" that K diffuse from plagioclase of unmelted parts to SMPs, since the spatial distances of unmelted parts and SMPs requires a millimeter to centimeter diffusion within a short time. Previous estimates of the cooling rate of melt veins span several orders of magnitude ranging from 5000 °C/s (Walton et al., 2006) to 0.2 °C/s (Beck et al., 2007) for millimeter melting veins. Suppose that the temperature of SMPs drops from 2500 °C down to 500 °C (Shaw and Walton, 2013), the cooling time would correspondingly be 0.4 s to 2.78 h. The calculated diffusion distances ($L = (Dt)^{1/2}$, where L is the diffusion distance; D is the diffusion coefficient, 3×10^{-8} cm^2/s under 1 GPa, adopted from Watson and Jurewicz (1984); and t is the diffusing time) are 1×10^{-4} cm for 0.4 s and 1.7×10^{-2}cm for 2.78 h. These distances are at least two orders of magnitude lower than the observed centimeter-scale migrating distances. In addition, there is no evident that the instantaneous high pressure can increase diffusive rate of K. Therefore, the "simple solid-melt diffusing model" alone cannot explain the K migration distance.

Here, we propose a scenario that tiny melts occurred initially at the interfaces of minerals and fractures upon the instantaneous impact. These tiny melts were chemically equal to the original minerals initially, and K would have the potential to diffuse into melts. Map scanning and line scanning of plagioclase also reveals K migration to shock fractures (Fig. 5 and Figs. S5, S6). Then these tiny melts merged and migrated under shock–induced pressure gradient. Elemental exchange occurred during the melt formation and migration, with incompatible elements preferentially diffused into melts. Diffusion-induced kinetic K isotope fractionation would enrich melts in light isotopes. Subsequently, these melts converged and were injected to the larger melt pockets. The migration of melts in shocked chondrites were studied and many petrological evidences have been found before (Tomkins et al., 2013; Fan et al., 2022). In our sample, the flow of melts is also observed (Figs. S1–S3). The diffusion induced elemental and isotopic variations for both melts and residual unmelted parts were calculated based on mass balance with method reported in Zhu et al. (2015) (see detailed calculation in the Supplementary Materials). The calculation results (Fig. 6) show that the measured K and K isotopic data lie on or near the modeling curves, indicating that diffusion could potentially produce the observed large K isotopic fractionation. Nonetheless, the detailed process of K diffusion merit further study and the formation of SMP could be more complicated than previous thought.

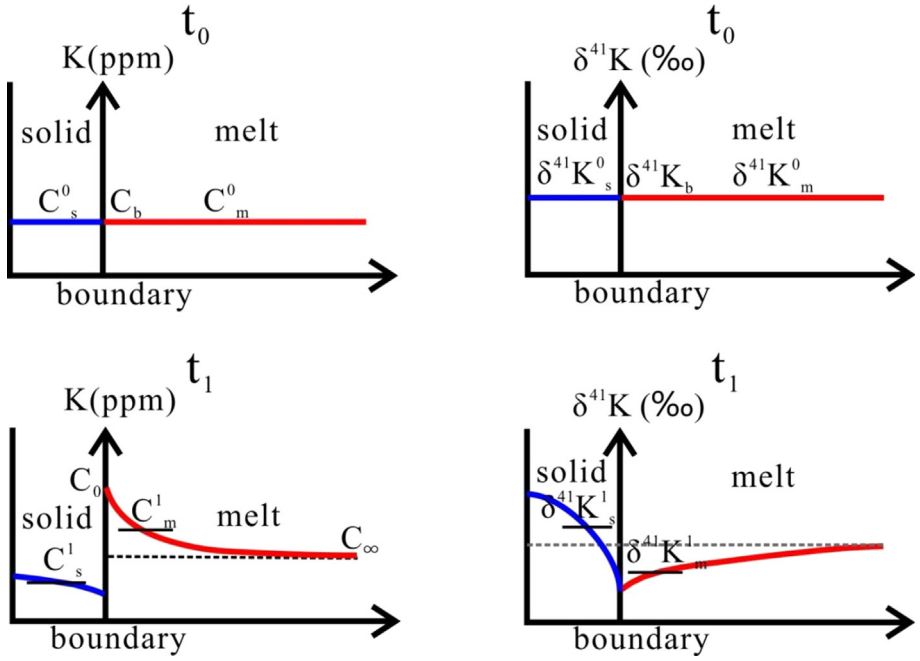

Fig. 4. Model for diffusion-caused K elemental variation and isotopic fractionations in solid and melt. t_0 is the starting time point of melting, when K and $\delta^{41}K$ in the solid (blue line) have the same values with those of melt phases (red line). t_1 is the time point that diffusion occurs. The K and $\delta^{41}K$ diffusing profiles of solid and melt parts are exhibited by blue and red curves. The black transverse lines represent the mean values. (For interpretation of the references to color in this figure legend, the reader is referred to the web version of this article.)

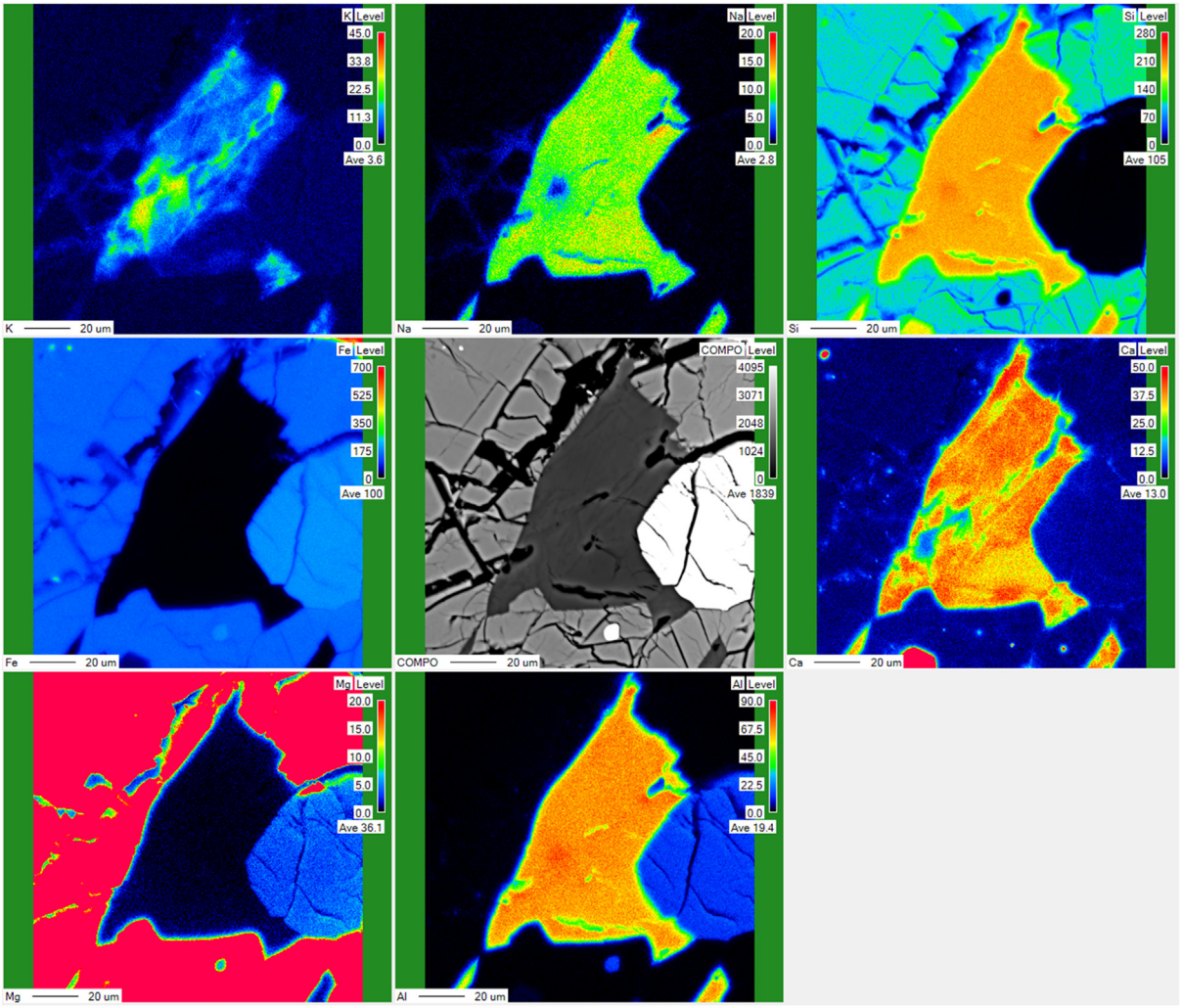

Fig. 5. Map scanning of plagioclase in unmelted parts of Viñales. K abundance in the shock fractures are higher than other areas, indicating K diffusing from normal areas to shock induced fractures.

4.2. Zn isotopic fractionation during heavy shocks

The SMPs have remarkably higher Zn isotopic values relative to the paired unmelted parts. Combined with the Zn content data (after Mg-normalization), it can be confirmed that the isotopic fractionation is related to Zn loss from SMPs. Two pathways are discussed below: (1) metal/sulphide segregation, or (2) Zn evaporation.

4.2.1. Zn isotopic fractionation during metal/sulphide segregation

The sequential dissolution experiment indicated that Zn is mostly hosted in silicate and sulphide phases with minor hosted in metals (Luck et al., 2005; Pringle et al., 2017). The distribution among the phases has been invoked as a mechanism for accounting for the variable Zn isotope composition of shock-melt meteorites. As an impact-melt event occurs, the metal/sulphide phase could re-accumulate into gravitational nodules and separate out of melts, which likely affects the Zn isotopic compositions of meteorites (Andronikov et al., 2015). However, Mahan et al. (2017) reported the metal-silicate Zn isotope fractionation to be between −0.05 ± 0.01‰ and 0.12 ± 0.04‰, regardless of whether the metal phase contained sulphur. It is in general accordance with the $\Delta^{66}Zn_{metal\text{-}silicate}$ values from Bridgestock et al. (2014), ranging from −0.14 ± 0.12‰ to 0.21 ± 0.15‰, which supports no substantial Zn metal-silicate isotope fractionation in high-temperature condition. Moreover, Zn also exhibits similar elemental partitioning between sulphide and silicate phases ($D_{sulphide\text{-}silicate}$ = 1), and no resolvable isotopic fractionation upon lunar sulphide extraction has been observed (Xia et al., 2019). Therefore, the observed ~0.8‰ Zn isotopic fractionation in this study is unlikely caused by metal/sulphide segregation.

4.2.2. Zn isotopic fractionation during evaporation

Impact induced Zn volatilization and isotopic fractionation were initially revealed in some lunar soil and basalt samples (Moynier et al., 2006; Herzog et al., 2009). Later, ureilites with variable shock degrees were studied and significant correlation between Zn isotopes and shock degrees was found (Moynier et al., 2010). Considering that the observed Zn isotopic fractionations are lower than that calculated with simple Rayleigh distillation, they suggested the evaporation occurred under a diffusion-limited situations in the ureilite parent body. Another similar study from Brugier et al. (2019) considers that the signature of Zn isotope composition is the result of evaporation processes, which is controlled by both high temperature of the ureilite parent body mantle and post-shock heating. Evidences of Zn evaporation were also found in terrestrial samples. For example, Kamber and Schoenberg (2020) reported Zn loss and isotope fractionation in

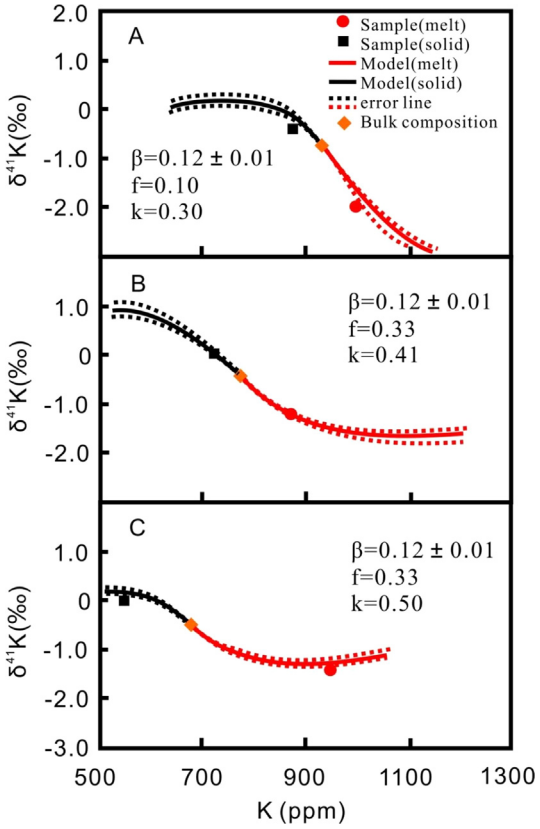

Fig. 6. Binary plot of K contents and K isotope compositions generated by solid-melt diffusion. (A)–(C) are simulation results for Chelyabinsk, Viñales and Tassédet 004 samples. Black solid curves represent the K and δ^{41}K coordinated variations caused by continuous diffusion in the solid phase, while red solid curves represent the K and δ^{41}K variations in the melt phase. The dashed curves represent the errors if β has slight alterations (±0.01). The orange diamonds are the initial points and they also represent the bulk rock compositions. Black squares and red circles are measured data of unmelted parts and SMPs, respectively. (For interpretation of the references to color in this figure legend, the reader is referred to the web version of this article.)

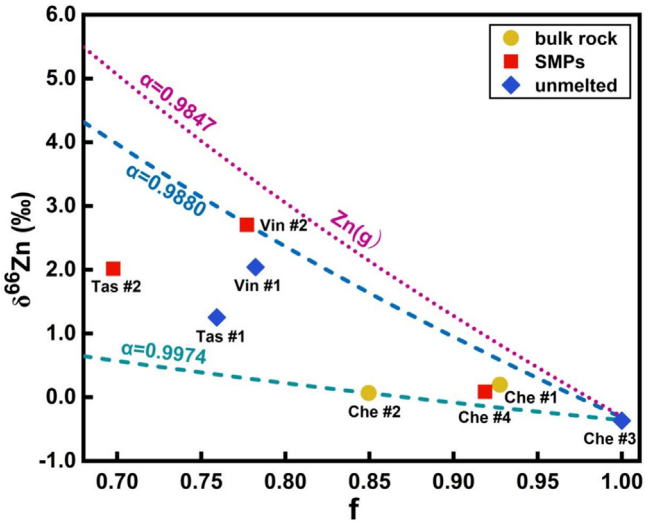

Fig. 7. Model of diffusion-limited Rayleigh distillation Zn isotopic variation. Pink dotted line (α = 0.9847) represents kinetic isotopic fractionation of Zn(g) in simple Rayleigh distillation. Blue dash line (α = 0.9880) and green dash line (α = 0.9974) were fitted by our measured Zn isotopic compositions. (For interpretation of the references to color in this figure legend, the reader is referred to the web version of this article.)

the melt sheet from the third-largest impact basin preserved on Earth and they attributed the results to the evaporation of impact melt. Mathur et al. (2021) observed volatilization-induced Zn loss and isotopic fractionation in sedimentary rock layers of the Cretaceous-Paleogene (K-Pg) boundary, which was formed by a large bolide impact. Our study of shocked ordinary chondrites showed comparably large Zn isotopic fractionation (~0.8‰) with the ureilites (~0.7‰), indicating the Zn loss from melts and its isotopic fractionation may also related to evaporation. In order to test the model, the calculation of Rayleigh distillation was performed. The unmelted part Che #3, which has the maximum Zn content of eight samples, was regarded as the initial material, and other seven samples were supposed to undergo various degree of evaporation loss. The δ^{66}Zn of residual materials were estimated by equation, $\delta_{final} = \delta_{initial} + \left[(1000 + \delta_{initial})\left(f^{\alpha-1} - 1\right)\right]$, where f is the remaining Zn fraction and α is fractionation factor. The calculation results are shown in Fig. 7. If the evaporation occurs under simple Rayleigh distillation, a larger isotope fractionation should be expected. Actually, our Zn isotopic data are consistent with the evaporation under diffusion-limited regime proposed by Moynier et al. (2010) and Sossi et al. (2020). Since the diffusion of Zn in the melts is insufficient to maintain Zn isotopic homogeneity within the melts, the evaporating Zn would not be as light as it occurs under the situation of simple Rayleigh distillation. In order to accommodate our Zn isotopic data, the fractionation factor was suppressed to 0.988 and 0.997. Summarily, the Zn isotopic fractionation probably results from diffusion-limited evaporation upon shock melting in the ordinary chondrites parent body.

4.3. The decoupling of K and Zn during shocks and its implications

The redistribution of volatile elements and kinetic isotope fractionations from heavy shock events was not fully understood before. Our study confirmed the K enrichment in SMPs and for the first time revealed extremely large K isotope fractionation associated with shock melting in ordinary chondrites. The K elemental and isotopic variations revealed in shock melting events are confined at small scale of the meteorites and hence are easy to be masked by whole-rock measurements. For example, the Che #2, which experienced shock melting and contain both melted and unmelted parts, has an identical K isotopic composition to the shock melting free fragment (Che #1). The reason that previous measurements of ordinary chondrites found no relation between K isotopes and shock levels (Bloom et al., 2020) might also attribute to this, yet it still need further investigation. Contrastively, the Zn isotopic measurements of melts and unmelted parts confirmed its volatilization from melts and indicated a diffusion-limited evaporation in shock melts, which is consistent with the previous study (Moynier et al., 2010).

Actually, similar decoupling behavior of K from Zn have been found in studying tektites and nuclear detonation materials (Day et al., 2017; Chen et al., 2019; Jiang et al., 2019). Both of the studies showed that K is prone to stay in melts and has significantly lower volatility than Zn and Cu. The reason for this could be either the difference in 50% T_c or binding with gaseous anions, e.g., S or Cl. Our results further reveal an opposite direction of elemental enrichment and reverse isotopic fractionation (Fig. 8) between K and Zn that during shock flash melting, with the behavior of K is controlled by incompatibility while Zn is governed by evaporation. Other alkaline MVEs (e.g., Li and Rb) seem to follow the behavior of K and enrich in melts, although the isotopic data is currently absent. Regardless the detailed mechanism and processes, the dramatic K isotope fractionation and decoupling from Zn isotopes further our understanding in high-temperature impacts and may

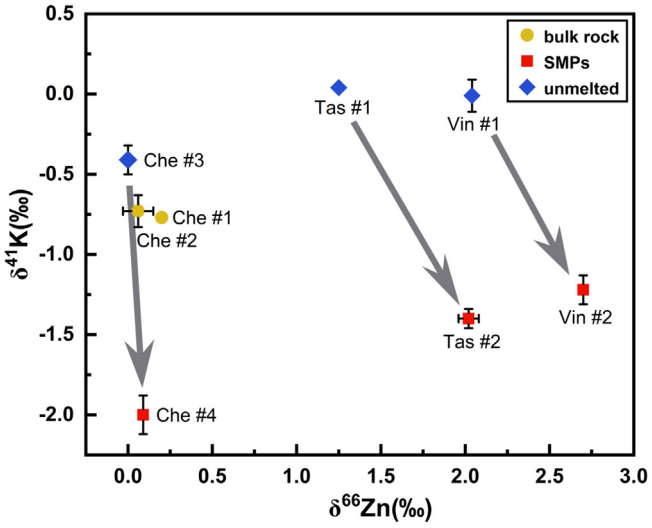

Fig. 8. The decoupling of K and Zn isotopic composition between melts and unmelted regions within the paired samples. All the melts (Che #4, Vin #2 and Tas #2) enrich in isotopically light K and heavy Zn, compared with the paired unmelted parts (Che #3, Vin #1 and Tas #1).

indicate a complicated history for heterogeneity of volatiles in solar system.

5. Summary

We studied K and Zn isotopes, whole-rock chemistry, petrology and mineralogy of eight shocked ordinary chondritic samples. All three SMPs show extremely lower K isotopic compositions ($\delta^{41}K$ = −1.99‰, −1.22‰ and −1.40‰) relative to adjacent unmelted parts ($\delta^{41}K$ = −0.41‰, −0.01‰ and 0.04‰). In contrast, Zn isotopic compositions of SMPs ($\delta^{66}Zn$ = −0.19‰, 2.42‰, 1.74‰) are heavier than paired unmelted parts ($\delta^{66}Zn$ = −0.65‰, 1.76‰, −0.97‰). Our results reveal a significant effect of shock melting on both K and Zn isotopes. Through comparison with Na and Li abundances in SMPs, it can be concluded that the observed K enrichment is governed by its incompatible affinity and the K migration is driven by melt-solid diffusion accompanying large kinetic isotope fractionation of K. We proposed a “tiny melt migration” to explain the large diffusing distance although the details need further study. Decoupling with K, the systematically loss of Zn and heavy Zn isotopes in melts are probably related to impact-induced evaporation under a diffusion-limited regime in the parent body. The remarkable K and Zn isotope fractionation between SMPs and unmelted parts promote our understanding of volatile isotope behaviors during impacts among asteroids and might indicate a complicated history for heterogeneous distribution of volatiles in solar system.

Declaration of Competing Interest

The authors declare that they have no known competing financial interests or personal relationships that could have appeared to influence the work reported in this paper.

Acknowledgments

We thank Fang-Zhen Teng, Yun Liu, Hui-Ming Bao, Run-Sheng Yin, Lie-Meng Chen, Hao Yan, Xin-Yang Chen and Tian-Yi Huang for comments on the writing. We also thank Hui-Yi Chen for providing the Tassédet 004 meteorite. Yan Hu provided help in the laboratory work and she also provided sanitizers and masks for members doing this work in the lab during the special COVID-19 period in March 2020. Reviews by Yang-Ting Lin, Frédéric Moynier and two anonymous referees helped shape the ideas. Editorial handling by Frédéric Moynier is acknowledged. This study is supported by Strategic Priority Research Program of Chinese Academy of Sciences (Grant No. XDB 41000000), Pre-research Project on Civil Aerospace Technologies (No. D020202) and National Natural ScienceFoundation of China (Grants 42073020, 42173046).

Appendix A. Supplementary material

Supplementary data to this article include: the Supplementary Text (the method of mass balance calculation), Figs. S1–S6 (petrology, mineralogy and elemental ratio of SMPs and unmelted parts, and K heterogeneous distribution within plagioclase), Table S1 (chemical compositions of bulk samples, minerals and glass) and References. Supplementary material to this article can be found online at https://doi.org/10.1016/j.gca.2023.03.031.

References

Aigner-Torres, M., Blundy, J., Ulmer, P., Pettke, T., 2007. Laser Ablation ICPMS study of trace element partitioning between plagioclase and basaltic melts: an experimental approach. Contrib. Mineral. Petrol. 153, 647–667.
Albarede, F., 2009. Volatile accretion history of the terrestrial planets and dynamic implications. Nature 461, 1227–1233.
Andronikov, A.V., Andronikova, I.E., Hill, D.H., 2015. Impact history of the Chelyabinsk meteorite: Electron microprobe and LA-ICP-MS study of sulfides and metals. Planet. Space Sci. 118, 54–78.
Barrat, J.A., Zanda, B., Moynier, F., Bollinger, C., Liorzou, C., Bayon, G., 2012. Geochemistry of CI chondrites: Major and trace elements, and Cu and Zn Isotopes. Geochim. Cosmochim. Acta 83, 79–92.
Beck, P., Ferroir, T., Gillet, P., 2007. Shock-induced compaction, melting, and entrapment of atmospheric gases in Martian meteorites. Geophys. Res. Lett. 34.
Bloom, H., Lodders, K., Chen, H., Zhao, C., Tian, Z., Koefoed, P., Peto, M.K., Jiang, Y., Wang, K., 2020. Potassium isotope compositions of carbonaceous and ordinary chondrites: Implications on the origin of volatile depletion in the early solar system. Geochim. Cosmochim. Acta 277, 111–131.
Bridgestock, L.J., Williams, H., Rehkämper, M., Larner, F., Giscard, M.D., Hammond, S., Coles, B., Andreasen, R., Wood, B.J., Theis, K.J., Smith, C.L., Benedix, G.K., Schönbächler, M., 2014. Unlocking the zinc isotope systematics of iron meteorites. Earth Planet. Sci. Lett. 400, 153–164.
Brugier, Y.A., Barrat, J.A., Gueguen, B., Agranier, A., Yamaguchi, A., Bischoff, A., 2019. Zinc isotopic variations in ureilites. Geochim. Cosmochim. Acta 246, 450–460.
Canup, R.M., 2004. Simulations of a late lunar-forming impact. Icarus 168, 433–456.
Chen, M., Goresy, A.E., 2000. The nature of maskelynite in shocked meteorites: not diaplectic glass but a glass quenched from shock-induced dense melt at high pressures. Earth Planet. Sci. Lett. 179, 489–502.
Chen, H., Nguyen, B.M., Moynier, F., 2013. Zinc isotopic composition of iron meteorites: Absence of isotopic anomalies and origin of the volatile element depletion. Meteorit. Planet. Sci. 48, 2441–2450.
Chen, H., Meshik, A.P., Pravdivtseva, O.V., Day, J.M.D., Wang, K., 2019. Potassium isotope fractionation during high-temperature evaporation determined from the Trinity nuclear test. Chem. Geol. 522, 84–92.
Ciesla, F.J., 2008. Radial transport in the solar nebula: Implications for moderately volatile element depletions in chondritic meteorites. Meteorit. Planet. Sci. 43, 639–655.
Daly, R.T., Schultz, P.H., 2018. The delivery of water by impacts from planetary accretion to present. Sci. Adv. 4, eaar2632.
Day, J.M.D., Moynier, F., 2014. Evaporative fractionation of volatile stable isotopes and their bearing on the origin of the Moon. Philos. Trans. R. Soc., A 372, 20130259.
Day, J.M., Moynier, F., Meshik, A.P., Pradivtseva, O.V., Petit, D.R., 2017. Evaporative fractionation of zinc during the first nuclear detonation. Sci. Adv. 3, e1602668.
Fan, Y., Li, S., Liu, S., Peng, H., Song, G., Smith, T., 2022. The distribution of the desert meteorites in China and their classification. Meteorit. Planet. Sci. 57, 683–701.
Fritz, J., Greshake, A., Fernandes, V.A., 2017. Revising the shock classification of meteorites. Meteorit. Planet. Sci. 52, 1216–1232.
Gargano, A., Sharp, Z., Shearer, C., Simon, J., Halliday, A., Buckley, W., 2020. The Cl isotope composition and halogen contents of Apollo-return samples. Proc. Natl. Acad. Sci. U.S.A. 117, 23418–23425.
Herzog, G.F., Moynier, F., Albarède, F., Berezhnoy, A.A., 2009. Isotopic and elemental abundances of copper and zinc in lunar samples, Zagami, Pele's hairs, and a terrestrial basalt. Geochim. Cosmochim. Acta 73, 5884–5904.
Hin, R.C., Coath, C.D., Carter, P.J., Nimmo, F., Lai, Y.J., Pogge Von Strandmann, P.A.E., Willbold, M., Leinhardt, Z.M., Walter, M.J., Elliott, T., 2017. Magnesium isotope evidence that accretional vapour loss shapes planetary compositions. Nature 549, 511–515.

Hu, Y., Chen, X.Y., Xu, Y.K., Teng, F.Z., 2018. High-precision analysis of potassium isotopes by HR-MC-ICPMS. Chem. Geol. 493, 100–108.
Hu, Y., Moynier, F., Bizzarro, M., 2022. Potassium isotope heterogeneity in the early Solar System controlled by extensive evaporation and partial recondensation. Nat. Commun. 13, 7669.
Humayun, M., Clayton, R.N., 1995. Potassium isotope cosmochemistry: genetic implications of volatile element depletion. Geochim. Cosmochim. Acta 59, 2131–2148.
Jiang, Y., Chen, H., Fegley, B., Lodders, K., Hsu, W.B., Jacobsen, S.B., Wang, K., 2019. Implications of K, Cu and Zn isotopes for the formation of tektites. Geochim. Cosmochim. Acta 259, 170–187.
Johnson, B.C., Walsh, K.J., Minton, D.A., Krot, A.N., Levison, H.F., 2016. Timing of the formation and migration of giant planets as constrained by CB chondrites. Sci. Adv. 2, e160165.
Kamber, B.S., Schoenberg, R., 2020. Evaporative loss of moderately volatile metals from the superheated 1849 Ma Sudbury impact melt sheet inferred from stable Zn isotopes. Earth Planet. Sci. Lett. 544, 116356.
Kato, C., Moynier, F., Valdes, M.C., Dhaliwal, J.K., Day, J.M.D., 2015. Extensive volatile loss during formation and differentiation of the Moon. Nat. Commun. 6, 7617.
Koefoed, P., Pravdivtseva, O., Ogliore, R., Jiang, Y., Lodders, K., Neuman, M., Wang, K., 2022. The Dynamic Formation Process of the CB Chondrite Gujba. Geochim. Cosmochim. Acta 332, 33–56.
Ku, Y., Jacobsen, S.B., 2020. Potassium isotope anomalies in meteorites inherited from the protosolar molecular cloud. Sci. Adv. 6, eabd0511.
Li, W.Q., Beard, B.L., Li, S.L., 2016. Precise measurement of stable potassium isotope ratios using a single focusing collision cell multi-collector ICP-MS. J. Anal. Atom. Spectrom. 31, 1023–1029.
Li, S.J., Leya, I., Wang, S.J., Smith, T., Bao, H.M., Fan, Y., Mo, B., 2021. Exposure history, petrology, and shock-induced sulfidization reaction of Alatage Mountain 001 strewn field samples. Meteorit. Planet. Sci. 56, 1293–1310.
Lodders, K., 2003. Solar system abundances and condensation temperatures of the elements. Astrophys. J. Lett. 591, 1220–1247.
Luck, J.M., Othman, D.B., Albarède, F., 2005. Zn and Cu isotopic variations in chondrites and iron meteorites: early solar nebula reservoirs and parent-body processes. Geochim. Cosmochim. Acta 69, 5351–5363.
Mahan, B., Siebert, J., Pringle, E.A., Moynier, F., 2017. Elemental partitioning and isotopic fractionation of Zn between metal and silicate and geochemical estimation of the S content of the Earth's core. Geochim. Cosmochim. Acta 196, 252–270.
Maréchal, C.N., Télouk, P., Albarède, F., 1999. Precise analysis of copper and zinc isotopic compositions by plasma-source mass spectrometry. Chem. Geol. 156, 251–273.
Mathur, R., Mahan, B., Spencer, M., Godfrey, L., Landman, N., Garb, M., Graham, P.D., Liu, S.A., Oboh-Ikuenobe, F.E., 2021. Fingerprinting the Cretaceous-Paleogene boundary impact with Zn isotopes. Nat. Commun. 12, 4128.
Moynier, F., Albarède, F., Herzog, G.F., 2006. Isotopic composition of zinc, copper, and iron in lunar samples. Geochim. Cosmochim. Acta 70, 6103–6117.
Moynier, F., Le Borgne, M., 2015. High precision zinc isotopic measurements applied to mouse organs. J. Vis. Exp. 99, e52479.
Moynier, F., Blichert-Toft, J., Luck, J.M., Telouk, P., Albare'de, F., 2007. Comparative stable isotope geochemistry of Ni, Cu, Zn, and Fe in chondrites and iron meteorites. Geochim. Cosmochim. Acta 71, 4365–4379.
Moynier, F., Beck, P., Jourdan, F., Yin, Q.Z., Reimold, U., Koeberl, C., 2009. Isotopic fractionation of zinc in tektites. Earth Planet. Sci. Lett. 277, 482–489.
Moynier, F., Beck, P., Yin, Q.Z., Ferroir, T., Barrat, J.A., Paniello, R., Telouk, P., Gillet, P., 2010. Volatilization induced by impacts recorded in Zn isotope composition of ureilites. Chem. Geol. 276, 374–379.
Moynier, F., Paniello, R.C., Gounelle, M., Albarède, F., Beck, P., Podosek, F., Zanda, B., 2011. Nature of volatile depletion and genetic relationships in enstatite chondrites and aubrites inferred from Zn isotopes. Geochim. Cosmochim. Acta 75, 297–307.
Moynier, F., Vance, D., Fujii, T., Savage, P., 2017. The isotope geochemistry of zinc and copper. Reviews in Mineralogy and Geochemistry 82, 543–600.
Nabiei, F., Badro, J., Dennenwaldt, T., Oveisi, E., Cantoni, M., Hebert, C., Goresy, A.E., Barrat, J.A., Gillet, P., 2018. A large planetary body inferred from diamond inclusions in a ureilite meteorite. Nat. Commun. 9, 1327.
Neuman, M., Holzheid, A., Lodders, K., Fegley, B., Jolliff, B.L., Koefoed, P., Chen, H., Wang, K., 2022. High temperature evaporation and isotopic fractionation of K and Cu. Geochim. Cosmochim. Acta 316, 1–20.
Nie, N.X., Chen, X.Y., Hopp, T., Hu, J.Y., Zhang, Z.J., Teng, F.Z., Shahar, A., Dauphas, N., 2021. Imprint of chondrule formation on the K and Rb isotopic compositions of carbonaceous meteorites. Sci. Adv. 7, eabl3929.
Paniello, R.C., Day, J.M.D., Moynier, F., 2012. Zinc isotopic evidence for the origin of the Moon. Nature 490, 376–379.
Pringle, E.A., Moynier, F., Savage, P.S., Badro, J., Barrat, J.A., 2014. Silicon isotopes in angrites and volatile loss in planetesimals. Proc. Natl. Acad. Sci. U.S.A. 111, 17029–17032.
Pringle, E.A., Moynier, F., 2017. Rubidium isotopic composition of the Earth, meteorites, and the Moon: Evidence for the origin of volatile loss during planetary accretion. Earth Planet. Sci. Lett. 473, 62–70.
Pringle, E.A., Moynier, F., Beck, P., Paniello, R., Hezel, D.C., 2017. The origin of volatile element depletion in early solar system material: Clues from Zn isotopes in chondrules. Earth Planet. Sci. Lett. 468, 62–71.
Savage, P.S., Moynier, F., Boyet, M., 2022. Zinc isotope anomalies in primitive meteorites identify the outer solar system as an important source of Earth's volatile inventory. Icarus 386, 115172.
Shaw, C.S.J., Walton, E., 2013. Thermal modeling of shock melts in Martian meteorites: Implications for preserving Martian atmospheric signatures and crystallization of high-pressure minerals from shock melts. Meteorit. Planet. Sci. 48, 758–770.
Sossi, P.A., Nebel, O., O'Neill, H., St, C., Moynier, F., 2018. Zinc isotope composition of the Earth and its behaviour during planetary accretion. Chem. Geol. 477, 73–84.
Sossi, P.A., Moynier, F., Treilles, R., Mokhtari, M., Wang, X., Siebert, J., 2020. An experimentally-determined general formalism for evaporation and isotope fractionation of Cu and Zn from silicate melts between 1300 and 1500 °C and 1 bar. Geochim. Cosmochim. Acta 288, 316–340.
Steller, T., Burkhardt, C., Yang, C., Kleine, T., 2022. Nucleosynthetic zinc isotope anomalies reveal a dual origin of terrestrial volatiles. Icarus 386, 115171.
Stoffler, D., Keil, K., Scott, E.R.D., 1991. Shock metamorphism of ordinary chondrites. Geochim. Cosmochim. Acta 55, 3845–3867.
Tian, Z., Chen, H., Fegley, B., Lodders, K., Barrat, J.A., Day, J.M.D., Wang, K., 2019. Potassium isotopic compositions of howardite-eucrite-diogenite meteorites. Geochim. Cosmochim. Acta 266, 611–632.
Tian, Z., Jolliff, B.L., Korotev, R.L., Fegley, B., Lodders, K., Day, J.M.D., Chen, H., Wang, K., 2020. Potassium isotopic composition of the Moon. Geochim. Cosmochim. Acta 280, 263–280.
Tian, Z., Magna, T., Day, J.M.D., Mezger, K., Scherer, E.E., Lodders, K., Hin, R., Koefoed, P., Bloom, H., Wang, K., 2021. Potassium isotope composition of Mars reveals a mechanism of planetary volatile retention. Proc. Natl. Acad. Sci. U.S.A. 118. e2101155118.
Tomkins, A.G., Weinberg, R.F., Schaefer, B.F., Langendam, A., 2013. Disequilibrium melting and melt migration driven by impacts: Implications for rapid planetesimal core formation. Geochim. Cosmochim. Acta 100, 41–59.
Wai, C.M., Wasson, J.T., 1977. Nebular condensation of moderately volatile elements and their abundances in ordinary chondrites. Earth Planet. Sci. Lett. 36, 1–13.
Walton, E., Shaw, C., Cogswell, S., Spray, J., 2006. Crystallization rates of shock melts in three martian basalts: Experimental simulation with implications for meteoroid dimensions. Geochim. Cosmochim. Acta 70, 1059–1075.
Wang, K., Jacobsen, S.B., 2016a. Potassium isotopic evidence for a high-energy giant impact origin of the Moon. Nature 538, 487–490.
Wang, K., Jacobsen, S.B., 2016b. An estimate of the Bulk Silicate Earth potassium isotopic composition based on MC-ICPMS measurements of basalts. Geochim. Cosmochim. Acta 178, 223–232.
Wang, Z.Z., Liu, S.A., Liu, J., Huang, J., Xiao, Y., Chu, Z.Y., Zhao, X.M., Tang, L.M., 2017. Zinc isotope fractionation during mantle melting and constraints on the Zn isotope composition of Earth's upper mantle. Geochim. Cosmochim. Acta 198, 151–167.
Wasson, J.T., Chou, C.L., 1974. Fractionation of moderately volatile elements in ordinary chondrites. Meteoritics 9, 69–84.
Watson, E.B., Jurewicz, S.R., 1984. Behavior of alkalies during diffusive interaction of granitic xenoliths with basaltic magma. The Journal of Geology 92, 121–131.
Wetherill, G., 1980. Formation for the terrestrial planets. Annu. Rev. Astron. Astrophys 18, 77–113.
Xia, Y., Kiseeva, E.S., Wade, J., Huang, F., 2019. The effect of core segregation on the Cu and Zn isotope composition of the silicate Moon. Geochemical perspectives letters 12, 12–17.
Xu, Y.K., Hu, Y., Chen, X.Y., Huang, T.Y., Sletten, R.S., Zhu, D., Teng, F.Z., 2019. Potassium isotopic compositions of international geological reference materials. Chem. Geol. 513, 101–107.
Yang, C., Liu, S.A., Zhang, L., Wang, Z.Z., Liu, P.P., Li, S.G., 2021. Zinc isotope fractionation between Cr-spinel and olivine and its implications for chromite crystallization during magma differentiation. Geochim. Cosmochim. Acta 313, 277–294.
Yang, Z., Song, W., Wen, H., Zhang, Y., Fan, H., Wang, F., Li, Q., Yang, T., Zhou, Z., Liao, S., Zhu, C., 2022. Zinc, cadmium and sulphur isotopic compositions reveal biological activity during formation of a volcanic-hosted massive sulphide deposit. Gondwana Research 101, 103–113.
Yin, F., Dai, D., 2021. Petrology and mineralogy of the Viñales meteorite, the latest fall in Cuba. Science Progress 104, 1–12.
Yu, Y., Hewins, R.H., Alexander, C.M.O., Wang, J., 2003. Experimental study of evaporation and isotopic mass fractionation of potassium in silicate melts. Geochim. Cosmochim. Acta 67, 773–786.
Zhao, C., Lodders, K., Bloom, H., Chen, H., Tian, Z., Koefoed, P., Peto, M.K., Wang, K., 2020. Potassium isotopic compositions of enstatite meteorites. Meteorit. Planet. Sci. 55, 1404–1417.
Zhu, D., Bao, H.M., Liu, Y., 2015. Non-traditional stable isotope behaviors in immiscible silica-melts in a mafic magma chamber. Sci. Rep. 5, 17561.
Zhu, C., Liao, S., Wang, W., Zhang, Y., Yang, T., Fan, H., Wen, H., 2018. Variations in Zn and S isotope chemistry of sedimentary sphalerite, Wusihe Zn-Pb deposit, Sichuan Province, China. Ore Geology Reviews 95, 639–648.